

# Performance of Water-based Liquid Scintillator

D. Beznosko<sup>c</sup>, M.V. Diwan<sup>a</sup>, S.Hans<sup>b</sup>, D. Jaffe<sup>a</sup>, S.H. Kettell<sup>a</sup>, R.Rosero<sup>b</sup>,  
H. Themann<sup>a</sup>, B. Viren<sup>a</sup>, E. Worcester<sup>a</sup>, M. Yeh<sup>b</sup>, C. Zhang<sup>a</sup>

<sup>a</sup>*Physics Department, Brookhaven National Laboratory, Upton, NY 11973, USA*

<sup>b</sup>*Chemistry Department, Brookhaven National Laboratory, Upton, NY 11973, USA*

<sup>c</sup>*Department of Physics, Nazarbayev University, Astana, 010000, KZ*

---

## Abstract

The Water-based Liquid Scintillator (WbLS) is a new material currently under development. It is based on the idea of dissolving the organic scintillator in water using special surfactants. This material strives to achieve the novel detection techniques by combining the Cerenkov rings and scintillation light, as well as the total cost reduction compared to pure liquid scintillator (LS).

Presented are the light yield measurements for the three different proton beam energies (210MeV, 475MeV and 2000MeV) for water, two different WbLS formulations (0.4% and 0.99%) and pure LS. The results show that a goal of 100 optical photons/MeV, indicated by the simulation to be an optimal light yield for observing both the Cerenkov ring and scintillation light from the proton decay in a large water detector, has been achieved.

*Keywords:* Water based, liquid scintillator, beam test

---

## 1. Motivation

In large water detectors, the Cerenkov radiation produced by a charged particle above the threshold can be used for particle identification, and the reconstruction of its direction and energy [1]. However, all charged particles below the Cerenkov threshold are missed. Detecting these below-threshold particles is important for various applications. For example, in the search of the proton decay, in the  $p^+ \rightarrow K^+ \bar{\nu}$  channel, where  $K^+$  is mostly below Cerenkov threshold and is invisible in a water detector. The use of the WbLS

---

*Email address:* `dima@dozory.us` (D. Beznosko)

9 makes the kaon visible and allows for the separation of  $K^+$ ,  $\mu^+$  and  $e^+$  signals  
10 using timing and reduce background for this decay channel.

11 In either LS or WbLS, the isotropic scintillation light is produced by  
12 the charged particle energy deposition via ionization, but the scintillator  
13 components may interfere with the Cerenkov ring detection. To detect  $K^+$   
14 and preserve the Cerenkov ring, MC studies indicate that the light yield  
15 (LY) from the scintillator component in the WbLS should be 100 optical  
16 photons/MeV.

17 Thus, WbLS potentially combines both the Cerenkov ring and scintil-  
18 lation light capabilities. It can preserve the particle identification for the  
19 particles above the Cerenkov threshold, and detect the charged particles be-  
20 low the threshold via the scintillation light. In addition, WbLS features the  
21 lower cost than pure LS and it is safer to handle[ask Minfang for reference].

22 The ability to reach the desired LY can be checked using the mono-  
23 energetic proton beam with different WbLS concentrations. For the test,  
24 the two different WbLS formulations (0.4% and 0.99%), pure water and pure  
25 LS samples were chosen. Three different proton beam energies were used  
26 with each sample. The choice of the energies comes from the following con-  
27 siderations:

- 28 • 2000MeV protons behave as minimum ionizing particle (MIP)
- 29 • 475MeV protons are just below the Cerenkov limit in water
- 30 • 210MeV protons have  $\sim$ same energy deposition as  $K^+$  from the proton  
31 decay channel mentioned above.

## 32 2. Experimental Setup

33 The experimental setup used for the proton beam test is shown in (Fig-  
34 ure 1). Two tubs with the samples were used (T1 and T2). Three 2cm x  
35 2cm 5mm thick plastic scintillator hodoscopes were used (H1 to H3) with the  
36 beam trigger being formed by the coincidence of the H1&H2 only. H3 was  
37 intended to verify whether particles exit T2. .

### 38 2.1. Tub and Signal Readout Description

39 Two tubs were used in the experiment:

- 40 • T1 from Polytetrafluoroethylene (PTFE) (white, highly reflective),

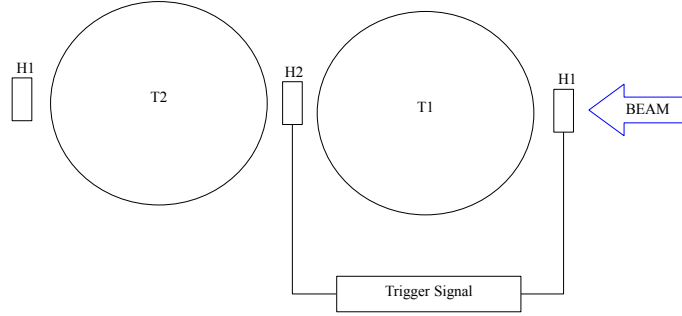


Figure 1: Proton beam test experimental setup.

- T2 from Aluminum, coated with black PTFE (very low reflectivity).

The T1 allows the capture of most of the light produced in the tub, whereas T2 allows for the observation of the light coming directly from the scintillation without the multiple wall reflections. An image of a tub is in (Figure 3). Both T1 and T2 have the same dimensions:

- the lid is 19.05mm thick,
- the walls and bottom are 6.35mm thick,
- inner height and diameter are 150mm.

. A detailed setup readout scheme is shown in (Figure 2). Both tubs were read out by Hamamatsu [2] R7723 2" Photo-multiplier tubes (PMT). An acrylic window transparent for the ultraviolet light (UVT) was used as a partition between the PMT and the liquid in the tub. The window was protruding through the lid and into the liquid by several millimeters to ensure that there are no air bubbles on its surface.

A readout was by the 4-channel 14bit CAEN [3] V1729A Flash Analog-to-Digital Converter (FADC). All tubs signals were connected to the FADC via a

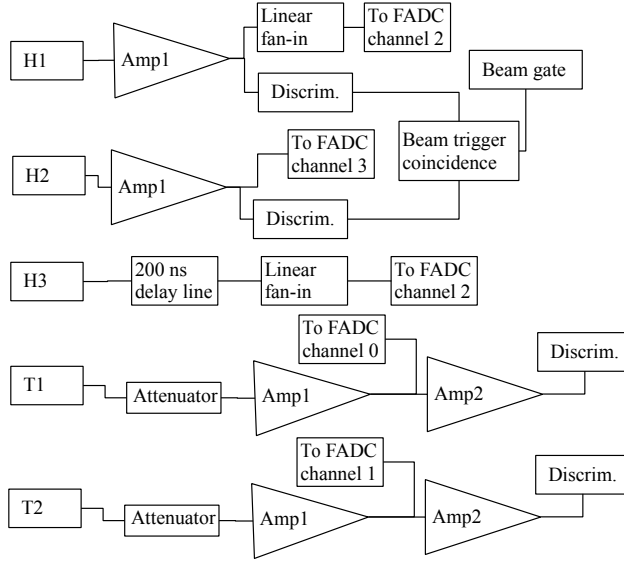


Figure 2: Proton beam test experimental setup.

variable attenuation unit (Phillips Scientific [4] 804) and a variable amplifier unit (Phillips Scientific 778). For the T1 and the T2 readouts, the gain was set to the values of  $\sim 2x$ . The first output from the amplifier goes to the FADC, with a dedicated channel for each tub. The second output from each amplifier channel was used for the single photo-electron (PE) calibration. The gain for the second amplification stage was set at  $\sim 10x$ .

All hodoscopes also were connected via  $\sim 2x$  gain amplifier channels that allows signal splitting. H1 and H3 shares the same FADC channel with latter signal being delayed by 200ns. H2 was connected to the last remaining channel of the FADC.

## 2.2. Triggering Scheme

Triggering schema was realized using three 2cm x 2cm, 5mm thick plastic scintillator counters that were readout by 2" PMTs via an air waveguide in order to remove the PMTs from direct beam exposure. The signal from the front-most and a middle counters were used to form a beam trigger, as indicated in the (Figure 2)

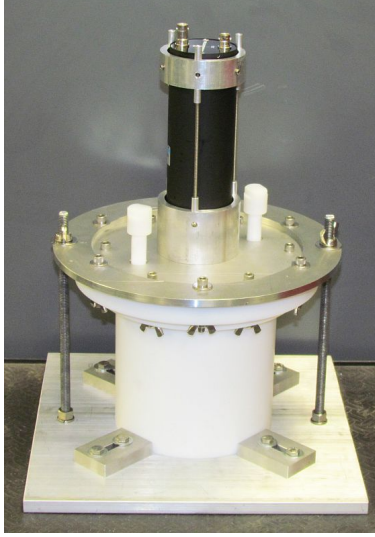


Figure 3: PTFE tub detector with a PMT.

### 2.3. Proton Beamline Description

A proton test beam was conducted at NASA Space Radiation Laboratory (NSRL) facility at BNL. As described above, the three proton beam energies were used: 210MeV, 475MeV and 2GeV. The beam had the following main characteristics:

- intensity of  $\sim 1\text{p+}/\text{bunch}$ ,
- beam size was  $1\text{cm} \times 1\text{cm}$  at 2GeV and  $5.4\text{cm} \times 5.4\text{cm}$  at 210MeV,
- 0.4s long spills every  $\sim 4$  sec.

## 3. Data Analysis

### 3.1. Liquids Measured

### 3.2. Waveform Analysis

The PMT signal is acquired as a waveform shown in (Figure 4). Total acquisition window is 2560 bins per event with each bin being 1ns wide; the signal is approximately centered and the approximate position is known beforehand. A 300ns window (central one in the figure, between the red and blue lines) is used to obtain the integrated signal area by summation. Each

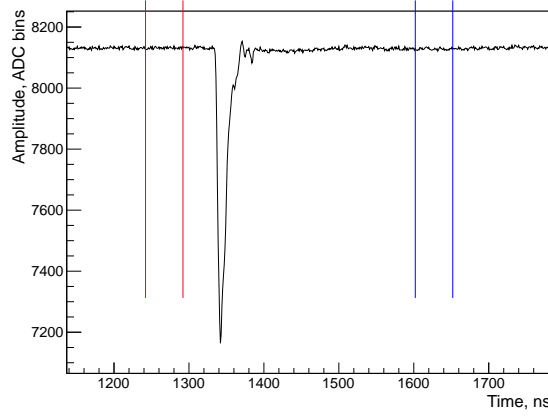


Figure 4: Typical PMT waveform with baseline check windows.

90 point is subtracted from the average baseline to achieve a positive sum. A  
 91 typical signal is smaller than the chosen window width, however, there is a  
 92 small spread in timing of the signals and we want' to be sure that all of the  
 93 signal has been integrated. The size of the chosen window is the same for all  
 94 samples and measurements.

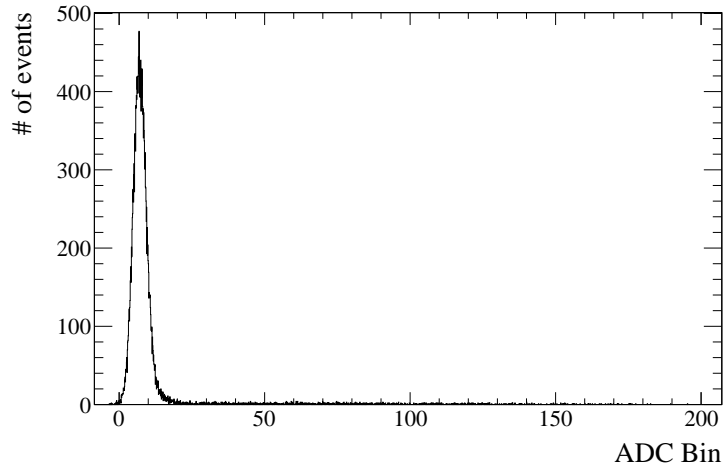


Figure 5: Typical baseline value for a single channel.

95 A baseline is defined as the average value of all the points in the first  
 96 integration window (between the two red lines) that is 50ns wide. A typical

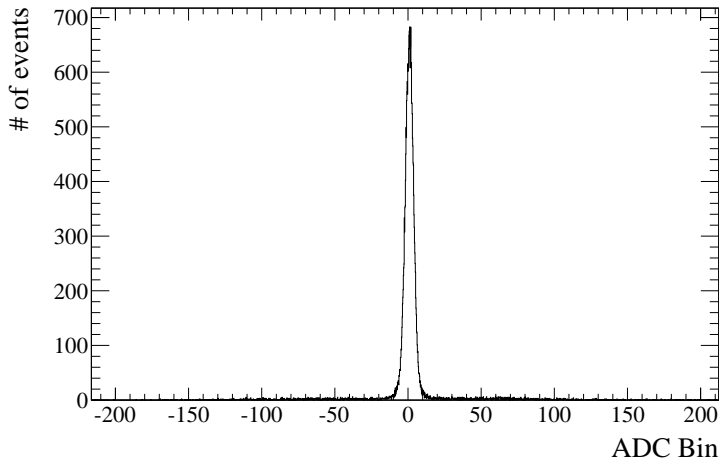


Figure 6: Difference between the baseline and the average of the post-signal window.

97 baseline is shown in (Figure 5) To check the baseline quality, its averaged  
 98 value is compared against the average of the post-signal window (between  
 99 two blue lines). This difference is illustrated in (Figure 6). Events with this  
 100 difference larger then  $\sim 20$  ADC bins are flagged as bad. This allows for the  
 101 removal of the noise events or events with the bad baseline. Additionally, a  
 102 comparison of the baseline with an average of a window at the very beginning  
 103 of the waveform (between 10ns and 40ns, not shown because the figure is  
 104 zoomed around the signal area) is used for general baseline quality check  
 105 using the above criterion.

106 The integrated area is a measure of total charge that can be converted  
 107 to the PE yield using the single PE calibration of the PMTs. This allows  
 108 to describe the measured signals independent of the hardware differences  
 109 between the channels.

110 The trigger information that is saved in the two additional FADC channels  
 111 allows for the offline trigger requirements be used.

### 112 3.3. Single Photo Electron Calibration

113 A single PE calibration was conducted for both signal channels at the end  
 114 of the test beam run. For it, the trigger is produced from the discriminator  
 115 that follows the second amplifier for the T1 and T2 signals (separately for  
 116 each, see Figure 2). The discriminator is set to  $\sim 1/10^{\text{th}}$  of the single PE  
 117 amplitude as to allows for better PE signal detection efficiency than using

118 random trigger. Additionally, this forces the PE signal to the signal window  
 119 region of the FADC output for the simplified analysis and elimination of the  
 120 partially captured signals. Note that a PE signal is much narrower and lower  
 121 in amplitude/area than the beam signals that are typically many PEs that  
 122 arrive with time distribution, thus a smaller integration window is used to  
 123 reduce noise for cleaner calibration (50ns instead of 300ns).

124 The signal area calibration is  $168.0 \pm 1.2$  ADC bins and  $132.9 \pm 1.6$  ADC  
 125 bins for T1 and T2 respectively (the PE signal is summed within the window,  
 126 so the unit of ADC bin is still used). A special care was taken to separately  
 127 verify that this method yields the same calibration values as using the light-  
 128 emitting diode (LED) scheme. For that, calibration runs using the described  
 129 above scheme and using the dim LED pulses were compared to each other.  
 130 The LED light level is chosen such that only  $\sim 1/10^{\text{th}}$  of the events has the  
 131 single PE signal to insure that these are the single photon detection responses.

### 132 3.4. *Light Yield Analysis*

133 The analysis process involves establishing the data quality selection cri-  
 134 teria, data fitting, interpretation of the fitting results and the evaluation of  
 135 the systematic errors. Each step is included within this chapter.

#### 136 3.4.1. *Data quality selection*

137 The data quality selection is done as a single step before the data is  
 138 analyzed. The care was taken to choose the criteria that do not introduce a  
 139 bias into the selection. These are:

- 140 • offline double trigger requirement for H1 and H2 to be above  $\sim 50\text{mV}$   
 141 and within the expected time window,
- 142 • baseline quality check as outlines in chapter 3.2,
- 143 • ADC saturation check for H1 and H2.

144 Each check is intended to remove potential noise or multiple particles  
 145 in an event. The saturation check indicates if several particles have passed  
 146 through the hodoscopes in a same beam spill that happens rarely at the  
 147 intensity used.



### 148 3.5. Light Yield Results

149 For each sample and energy, a histogram of the signal areas is computed.  
 150 A fit using a Gaussian and a bin likelihood method is then performed. The  
 151 fitting is done in two steps - first, a Gaussian is fitted in the range between the  
 152 half of the maximum peak values to obtain the first approximation. Then,  
 153 the fits around the found mean with  $1$ ,  $1.5$  and  $2\sigma$  are carried. This is done  
 154 to estimate the uncertainty that the fit width is adding because of the second  
 155 peak due to the two particles passing through the tub during the same trigger  
 156 time. Figure 3.5 shows the  $1.5\sigma$  fit of the single particle fit, and the two-  
 157 particle peak is visible on it as well. This plot is in the ADC bins for clarity;  
 158 single-PE calibration will be applied to all further plots.

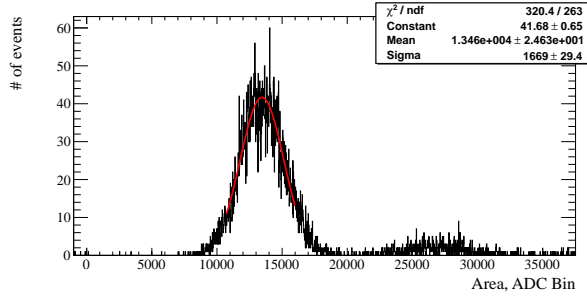


Figure 7: A sample fit of a tub signal.

159 The data for all the samples at all energies is then processed in the same  
 160 way. Plots in Figure 3.5 and in Figure 3.5 show the light yield results in PE  
 161 for the different samples and beam energies for Tub1 and tub2 respectively.

### 162 3.6. Energy deposition

163 In order to estimate the PE/MeV light yield of each sample, the energy  
 164 deposition in each sample is needed. Two methods were used for this pur-  
 165 pose: a GEANT4 simulation of the beamline setup with the deposition being  
 166 the mean of the 1000runs at each energy, and a simplified code that would  
 167 calculate the proton energy loss along a straight line path through the tubs  
 168 and hodoscopes with small steps, using the proton stopping power and range  
 169 tables (PSTAR) from the National Institute of Standards and Technology  
 170 (NIST). The WbLS was modeled as water, and the LS as toluene.

171 The resulting energy depositions are listed in Table 1. The difference  
 172 between the two methods is taken as the uncertainty for the values obtained.

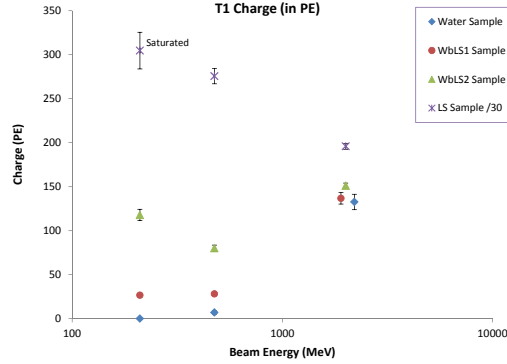


Figure 8: The light yield in PE for T1. At 2GeV beam energy, some points are offset for clarity.

### 173 3.7. Systematics

#### 174 3.7.1. Calibration Stability

## 175 4. Conclusion

## 176 References

- 177 [1] M. Fechner et.al. (The Super-Kamiokande Collaboration), ‘Kinematic re-  
178 construction of atmospheric neutrino events in a large water Cherenkov  
179 detector with proton identification’, Phys. Rev. D 79 (2009) 112010,  
180 arXiv:0901.1645
- 181 [2] Hamamatsu Photonics, 314-5 Shimokanzo, Toyooka-village, Iwatagun,  
182 Shizuoka-ken, 438-0193 Japan; <http://www.hamamatsu.com>
- 183 [3] CAEN (Costruzioni Apparecchiature Elettroniche Nucleari S.p.A.), Via  
184 della Vetraria 11, 55049 Viareggio, Province of Lucca, Italy, 0584 388398.
- 185 [4] Phillips Scientific, 31 Industrial Ave. Suite 1, Mahwah, N.J. 07430

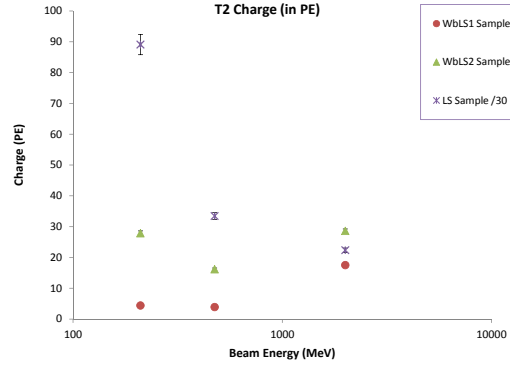


Figure 9: The light yield in PE for T2.

Table 1: Energy Deposition in Samples

Beam Energy (MeV)	Sample	T1 Energy Deposit (MeV)	T2 Energy Deposit (MeV)
210	Water, WbLS	70	113
	LS	59	124
475	Water, WbLS	39	42
	LS	34	36
2000	Water, WbLS	28	28
	LS	24	24